Measurement of the Electric Fluctuation Spectrum of Magnetohydrodynamic Turbulence

S. D. Bale,[1] P. J. Kellogg,[2] F. S. Mozer,[1] T. S. Horbury,[3] and H. Reme[4]

[1]*Department of Physics and Space Sciences Laboratory, University of California, Berkeley, California 94720, USA*
[2]*School of Physics and Astronomy, University of Minnesota, Minneapolis, Minnesota 55455, USA*
[3]*The Blackett Laboratory, Imperial College, London SW7 2BW, United Kingdom*
[4]*CESR, 31400 Toulouse, France*

(Received 23 February 2005; published 2 June 2005)

Magnetohydrodynamic (MHD) turbulence in the solar wind is observed to show the spectral behavior of classical Kolmogorov fluid turbulence over an inertial subrange and departures from this at short wavelengths, where energy should be dissipated. Here we present the first measurements of the electric field fluctuation spectrum over the inertial and dissipative wave number ranges in a $\beta \gtrsim 1$ plasma. The $k^{-5/3}$ inertial subrange is observed and agrees strikingly with the magnetic fluctuation spectrum; the wave phase speed in this regime is shown to be consistent with the Alfvén speed. At smaller wavelengths $k\rho_i \geq 1$ the electric spectrum is enhanced and is consistent with the expected dispersion relation of short-wavelength kinetic Alfvén waves. Kinetic Alfvén waves damp on the solar wind ions and electrons and may act to isotropize them. This effect may explain the fluidlike nature of the solar wind.

DOI: 10.1103/PhysRevLett.94.215002 PACS numbers: 52.35.Ra, 52.35.Bj

Turbulence is ubiquitous in astrophysical plasmas; turbulent processes are thought to a play role in cosmic ray and energetic particle acceleration and scattering [1], advection dominated accretion flows, and perhaps solar/stellar wind acceleration. Yet key aspects of the physics of turbulence in magnetized plasmas are poorly understood, in particular, the physics of dissipation at small scales. The classical scenario of magnetohydrodynamic turbulence is thus: fluctuations in the plasma are driven at some large ''outer'' scale and decay by interacting locally in k space. Eddies at some scale k exchange energy with eddies at nearby spatial scales, possibly as a three-wave or higher order interaction [2–4], with the resulting net flow of energy to smaller spatial scales (larger k); this cascade of energy occurs over an ''inertial subrange'' of k space and can be shown to predict a power spectrum that scales as $k^{-5/3}$. At the smaller scale of the ion thermal gyroradius, $k\rho_i \geq 1$, the ions become demagnetized and the plasma can no longer behave as a simple fluid; the turbulent energy is then thought to be damped on the thermal plasma by Landau or transit time damping. However, the details of this damping process are not known and there are few reported measurements in this regime of k space.

Observations of the magnetic spectrum show breakpoints near $k\rho_i \approx 1$, above which the magnetic spectrum typically becomes steeper [5–8]. This has been interpreted variously as evidence of kinetic Alfvén waves [5], whistler wave dispersion [9], and ion cyclotron damping of Alvén waves [10].

Here we report the first measured power spectrum of electric fluctuations in solar wind turbulence. The inertial subrange is clearly evident and follows the magnetic fluctuation spectrum. At large wave numbers $k\rho_i \geq 1$, the electric spectrum is enhanced.

Data are used from experiments on the Cluster spacecraft. Cluster flies four spacecraft, as a controlled tetrahedron, in an inclined orbit with apogee at 19 Earth radii (R_E). From December to May each year, the spacecraft exit the terrestrial magnetosphere on the dayside and make measurements in the solar wind. We use approximately 195 min of data during the interval 00:07:00–03:21:51 on 19 February 2002, when Cluster was at apogee and spent several hours in the ambient solar wind; all of our data are from Cluster spacecraft four.

The electric field is measured by the electric field and waves experiment (EFW) [11]; EFW is a double-probe experiment which measures the floating voltage of 8 cm diameter current-biased spheres extended on 44 m wires in quadrature. These spheres, as well as the spacecraft, are illuminated by the Sun and emit photoelectrons which cause the surfaces to charge positive with respect to the plasma. The surfaces attract a return current of thermal electrons which provide the electrical coupling to the plasma. Systematic variations in this coupling, due to changing illumination or variations in surface properties and work function, are a large source of background noise in EFW at the spacecraft spin period (4 sec) and harmonics. This is discussed more below. EFW measures the electric field on two orthogonal sensor pairs in the spacecraft spin plane at 25 samples/sec. These two components are rotated into X and Y components in the GSE (geocentric solar ecliptic) coordinate system. Since the GSE Y direction represents the orientation with best symmetry for solar illumination, this component of the electric field is generally less noisy; we use the GSE Y electric field E_y for all of our analysis. However, at any given instance, E_y is composed of data from all four electric field probes, each with slightly different photocoupling to the plasma. We therefore apply a finite impulse response filter to the data to notch out the primary perturbations at the spin tone and some harmonics.

The magnetic field is measured by the fluxgate magnetometer instrument [12]; three-component magnetic field vectors are sampled at 22 samples/sec. In our analysis, we use the GSE Z component of the magnetic field B_z for reasons that are explained below. Moments of the solar wind ion distribution (velocity, density, and temperature) are computed from the ion spectrum measured by the Cluster ion spectroscopy experiment [13].

Figure 1 shows an overview of the data used in the following analysis; panels (a) and (b) are wavelet spectrograms and will be discussed below. Panel (c) shows the two components of measured electric field E_x and E_y in GSE coordinates. Panel (d) show the magnetic field data. Panels (e), (f), and (g) show the plasma density, plasma ion β_i (ratio of plasma to magnetic pressure), and Alfvén Mach number. The average ion beta is $\bar{\beta}_i \approx 5$, average Alfvén speed $\bar{v}_A \approx 40$ km/s, and the average solar wind velocity is $\bar{v}_{\rm sw} \approx (-347, 4.9, -32.6)$ km/s (in GSE coordinates), over the entire interval. During the interval between 00:30 and 00:50, the magnetic field is nearly tangent to the Earth's bow shock (as per a calculation assuming straight field lines [14]); however, Cluster summary plots of electron and plasma wave data show *no* evidence of connection to the shock. All of our data are ambient solar wind.

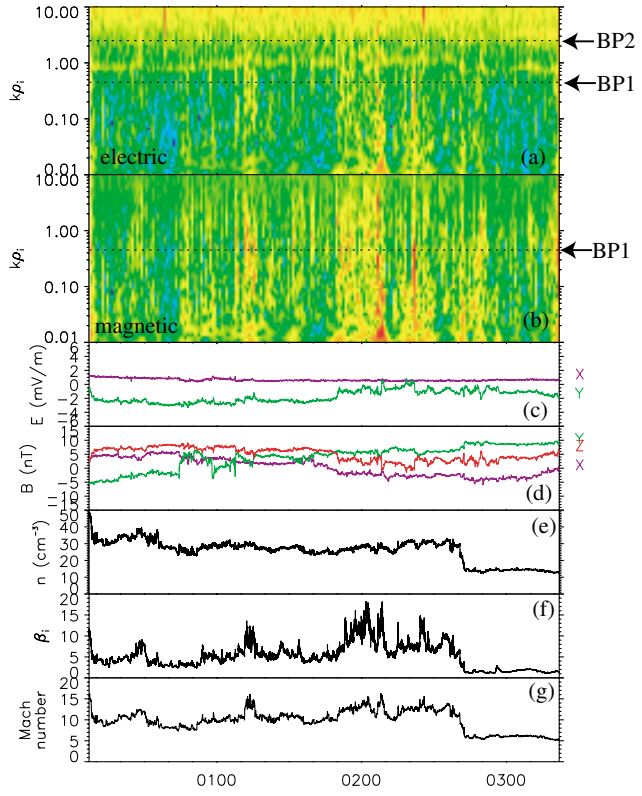

FIG. 1 (color). Wavelet and time series data of solar wind turbulence. From the top down, the five panels show (a) the wavelet spectrogram of E_y, as a function of $k\rho_i$, (b) a similar wavelet spectrogram of B_z, (c) the X and Y components of the measured electric field, (d) the vector magnetic field, (e) plasma ion density, (f) plasma ion β, and (g) the Alfvén Mach number. This entire interval was used for the spectral analysis of E_y and B_z. The spectral breakpoints are called out.

To compute power spectra, the electric field data E_y (25 samples/sec) were subsampled onto the time tags of the magnetic field data B_z (22 samples/sec) by linear interpolation; a total of exactly 2^{18} points are used. The power spectral density (PSD) was computed using both fast Fourier transform (FFT) and Morlet wavelet [15] schemes. The FFT was computed as follows: the data interval was divided into 64 contiguous ensembles of length 4096 (186 sec); this gives an inherent bandwidth of $\Delta f \approx 1/186$ Hz. To minimize spectral leakage, each ensemble was "whitened" by applying a first-order difference algorithm; the PSD was computed by FFT, then the spectrum was postdarkened [1] and divided by the bandwidth of the FFT. Since the data are prewhitened, no window function was applied before the FFT. The electric field spectra were then "cleaned" by interpolating over the narrow band spikes resulting from the spin-associated signals described above. A final spectrum was computed as the average of the 64 ensembles. Figure 2 shows the FFT power spectra of E_y and B_z (in black). Wavelet spectra were computed by first producing the (complex) FFT of E_y and applying the spectral cleaning (interpolation) to the real and imaginary parts, at positive and negative frequen-

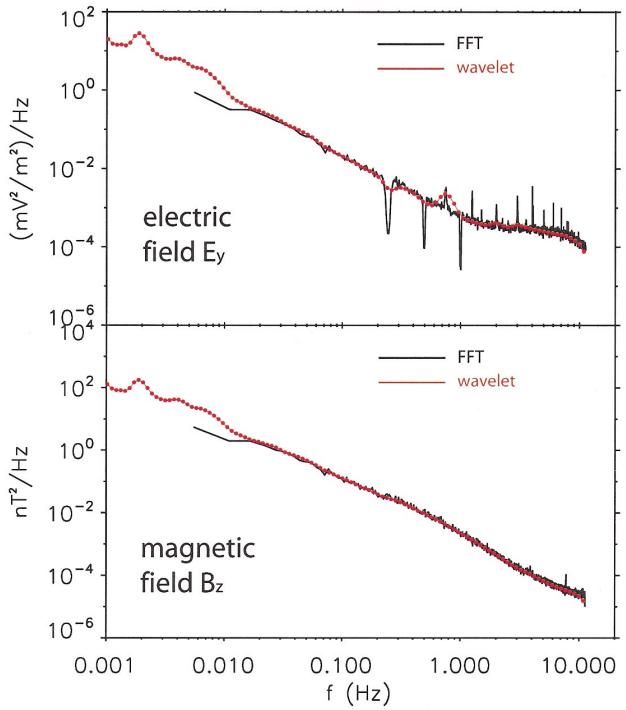

FIG. 2 (color). Power spectral density of electric δE_y and magnetic fluctuations δB_z as a function of frequency, computed from FFT (black) and Morlet wavelet (red) algorithms. The FFT spectrum of the electric field (upper panel) shows the effect of notch filters and residual spin-tone data.

cies. An inverse FFT restores the cleaned signal and a Morlet wavelet spectrogram was computed from this cleaned E_y, as well as the original B_z. The wavelet has 136 log-spaced frequencies; the final wavelet PSD is computed as the square of the spectrum averaged over time. The wavelet PSD is also shown in Fig. 2 (in red). The wavelet spectrum extends to lower frequencies than the FFT, which is composed of ensembles of smaller data intervals; however, these very low frequencies lie below the ''cone of influence'' and are unreliable [15]. Here we restrict our interpretation to the region where the FFT and wavelet spectra agree. The FFT electric spectrum in Fig. 2 shows clearly the effect of the notch filters and residual spin-harmonic spikes. The wavelet PSD, with its much larger bandwidth, mostly averages over these residual features although a depression near the notched portion of the spectrum can be seen. The FFT and wavelet PSD spectra agree remarkably well for both electric and magnetic fields.

Of course, our (human) scheme of measuring time means little to the solar wind plasma, so there is little reason to expect the data to be inherently organized by a power spectrum in Hertz. Since the solar wind is super-Alfvénic (Fig. 1), the phase speed v_A of the Alfvénic fluctuations is much less than the wind speed itself; hence the measured frequency spectrum is actually a Doppler-shifted wave number spectrum $\omega \approx k v_{\rm sw}$. This is often called Taylor's hypothesis and might not be considered to hold at large wave numbers, especially if waves are present with phase speeds greater than the solar wind speed (such as whistler waves).

As discussed above, it is considered that the fluidlike behavior of the wind breaks down at near $k\rho_i \approx 1$, therefore $k\rho_i$ is a natural parameter for organization of the power spectrum. The top panel of Fig. 3 shows the FFT and wavelet power spectra organized by $k\rho_i$, instead of frequency. For the FFT spectrum, the local values of $|v_{\rm sw}|$, T_i, and $|B|$ are used to compute $k = \omega/v_{\rm sw}$ and the thermal ion gyroradius $\rho_i = v_i/\Omega_{ci}$ averaged over each (186 sec) ensemble; the E_y and B_z power spectra are then interpolated onto a linearly spaced set of values $k\rho_i \in (0.006, 10)$. Since solar wind parameters vary slightly in each ensemble, this also has the effect of smearing (averaging) over the narrow band interference in the FFT PSD of E_y. The wavelet spectrograms are time averaged onto 4 sec intervals and then interpolated onto a set of log-spaced values of $k\rho_i$; panels (a) and (b) of Fig. 1 show these scaled spectrograms as a function of time. In Figs. 1(a) and 1(b), the fluctuation power has been divided by $k^{-5/3}$ to highlight fluctuations above the average spectrum of the inertial range. The electric and magnetic wavelet spectrograms are then averaged to compute the composite spectra in panel (a) of Fig. 3.

Between $k\rho_i \approx 0.015$ and 0.45, the wavelet and FFT spectra of electric and magnetic fluctuations show power law behavior with indices of $k^{-1.7}$, which is consistent with the Kolmogorov value of 5/3. Both δE_y and δB_z show breakpoints at near $k\rho_i \approx 0.45$; the magnetic spectrum becomes steeper with an index $k^{-2.12}$, while the electric spectrum becomes enhanced. As discussed above, steep magnetic spectra have been observed previously [6,8]. Above $k\rho_i \approx 0.45$, the electric spectrum is a power-law like $k^{-1.26}$ to $k\rho_i \approx 2.5$. Above this second breakpoint, an exponential $\exp(-k\rho_i/12.5)$ better fits the spectrum. At these higher wave numbers, the electric field data are noisy and show harmonics of the spin tone (as shown above). To test the validity of these data, we perform two analyses. The black dots of panel (c) in Fig. 3 show the correlation between the electric and the magnetic wavelet power as a function of $k\rho_i$. It can be seen that the fluctuations are strongly correlated through the inertial range (with coefficient ≈ 1), remain well correlated between the two break-

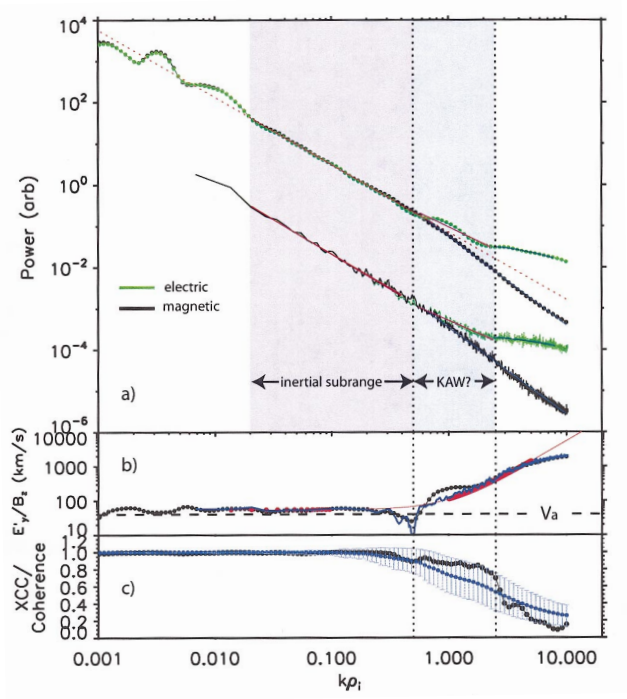

FIG. 3 (color). The wavelet (upper) and FFT (lower) power spectra of E_y (green) and B_z (black) binned as a function of wave number $k\rho_i$ (and offset for clarity) in panel (a). The electric spectra are multiplied by factors to lie atop the magnetic spectra. The spectrum is Kolmogorov $k^{-5/3}$ over the interval $k\rho_i \in (0.015, 0.45)$; a spectral breakpoint occurs for both E_y and B_z at $k\rho_i \approx 0.45$. A second breakpoint occurs for the electric spectrum at $k\rho_i \approx 2.5$ above which the electric spectrum is more exponential. Panel (b) shows the ratio of the electric to magnetic spectra in the plasma frame; the average Alfvén speed ($\bar{v}_A \approx 40$ km/s) is shown as a horizontal line. The red line is a fitted dispersion curve, discussed in the text. Panel (c) shows both the cross coherence of δE_y with δB_z (as blue dots with error bars) and the correlation between the electric and magnetic power (as black dots).

points $k\rho_i \in (0.45, 2)$, and begin to lose correlation quickly above the second breakpoint. A wavelet cross-spectral analysis (between δE_y and δB_z) was also computed; the blue bars show the cross-spectral coherence, with 1σ error bars, also as a function of $k\rho_i$. Again, δE_y and δB_z are strongly coherent through the inertial range and past the first breakpoint. We conclude that the electric and magnetic spectra are physical and well correlated up to the second spectral breakpoint. Above $k\rho_i \approx 2.5$ it is difficult to assess the quality of the data. If electrostatic waves are present, there is no expectation of correlation with δB; however, in this initial study, we cannot eliminate the possibility of systematic noise at these frequencies. Additionally, the effects of low pass filters on both the EFW and FGM experiments may modify the spectra at these highest ($k\rho_i > 3$) frequencies.

To estimate the phase speed of the fluctuations, we use Faraday's law and compute the ratio of the electric and magnetic spectra. Since the electric field measurements are made in the spacecraft (unprimed) frame, we need to Lorentz transform to the plasma (primed) frame by $\vec{E} = \vec{E}' + \vec{v}_{\rm sw} \times \vec{B}$. Panel (b) of Fig. 3 shows the phase speed

$$v_\phi(k\rho_i) = \frac{\delta E'_y(k\rho_i)}{\delta B_z(k\rho_i)} = \frac{\delta E_y(k\rho_i)}{\delta B_z(k\rho_i)} + \bar{v}_x - \bar{v}_z \frac{\bar{B}_x}{\bar{B}_z}, \quad (1)$$

where $\bar{v}_x$, $\bar{v}_z$, $\bar{B}_x$, and $\bar{B}_z$ are the average x and z components of the solar wind velocity and magnetic field. The ion data are sampled at 0.25 samples/sec; this necessitates using averages of $v_{\rm sw}$ in the Lorentz transformation. The black dots in panel (b) are computed from the wavelet spectrum, while the blue line is computed from the FFT spectrum. The average Alfvén speed $\bar{v}_A \approx 40$ km/sec is shown as a horizontal bar. Over, and even below, the inertial range $k\rho_i \in (0.015, 0.4)$, the phase speed is consistent with the local Alfvén speed; this is strong evidence of the Alfvénic nature of the cascade. The red curve in panel (b) is a fit of the function $v_0(1 + k^2\rho_i^2)$ to the FFT curve, where v_0 is a free parameter which finds a best fit at $v_0 \approx 55$ km/s. This function approximates the dispersion relation of kinetic Alfvén waves [16,17]. The cold-plasma whistler wave phase speed goes as $v_\phi \approx (k\rho_i)\beta^{-1/2}v_A$ above $\omega > \Omega_{ci}$, i.e., linear with $k\rho_i$, and would form a much shallower dispersion above $k\rho_i \approx 1$ than is observed in panel (b) of Fig. 3. This leads us to believe that the Alfvén waves in the inertial subrange eventually disperse as "kinetic" Alfvén waves above $k\rho_i \approx 1$, becoming more electrostatic and eventually damping on the thermal plasma. Plasma heating by linear dissipation of kinetic Alfvén waves at $\beta \approx 1$ has been studied in the context of accretion flows [16]. There it was found that Landau and transit time damping contribute to both proton and electron heating at short wavelengths, which is enhanced for higher β. Kellogg [18] computed the level of electric field fluctuations required to stochastically thermalize protons to 1 AU in the solar wind; he found that a spectral density of $E^2 \approx 10^{-11}$ V/m^2 Hz^{-1} was sufficient. This is 1 order of magnitude less than our observed levels (Fig. 2). It is, therefore, plausible to conclude that the observed electric spectrum is responsible for isotropizing the solar wind protons and may be the mechanism by which the solar wind maintains its fluidlike characteristics.

Cluster data analysis at UC Berkeley is supported by NASA Grant Nos. NAG5-11944 and NNG04GG08G.

[1] Bieber *et al.*, J. Geophys. Res. **98**, 3585 (1993).
[2] F. Waleffe, Phys. Fluids **4**, 350 (1992).
[3] P. Goldreich and S. Sridhar, Astrophys. J. **485**, 680 (1997).
[4] C. S. Ng and A. Bhattacharjee, Astrophys. J. **465**, 845 (1996).
[5] R. J. Leamon *et al.*, J. Geophys. Res. **104**, 22 331 (1999).
[6] R. J. Leamon *et al.*, J. Geophys. Res. **103**, 4775 (1998).
[7] M. L. Goldstein *et al.*, J. Geophys. Res. **99**, 11 519 (1994).
[8] H. J. Beinroth and F. M. Neubauer, J. Geophys. Res. **86**, 7755 (1981).
[9] O. Stawicki, S. P. Gary, and H. Li, J. Geophys. Res. **106**, 8273 (2001).
[10] S. P. Gary, J. Geophys. Res. **104**, 6759 (1999).
[11] G. Gustafsson *et al.*, Space Sci. Rev. **79**, 137 (1997).
[12] A. Balogh *et al.*, Space Sci. Rev. **79**, 65 (1997).
[13] H. Reme *et al.*, Space Sci. Rev. **79**, 303 (1997).
[14] P. C. Filbert and P. J. Kellogg, J. Geophys. Res. **84**, 1369 (1979).
[15] C. Torrence and G. P. Compo, Bull. Am. Meteorol. Soc. **79**, 61 (1998).
[16] E. Quataert, Astrophys. J. **500**, 978 (1998).
[17] S. R. Cranmer and A. A. van Ballegooijen, Astrophys. J **594**, 573 (2003).
[18] P. J. Kellogg, Astrophys. J **528**, 480 (2000).